Fire Technology (2025) 61:5445–5460
https://doi.org/10.1007/s10694-025-01789-9

Surface Flow Characterization of Fires Under the Combined Effect of Slope and Wind

Xingyu Ren[1,2] · Evan T. Sluder[1,4] · Michael V. Heck[1] · Torben P. Grumstrup[3] · Mark A. Finney[3] · Simo A. Mäkiharju[2] · Michael J. Gollner[1,2]

Received: 3 November 2024 / Accepted: 17 July 2025 / Published online: 8 August 2025
© The Author(s) 2025

Abstract
During wildland fire spread both slope and wind act together to modify fire dynamics, commonly accelerating the rate of fire spread. To investigate this coupling effect, flow field measurements were conducted on stationary gaseous fires produced over a tilt table in a wind tunnel, with fireline intensities ranging from 41 to 123 kW/m. The angle of inclination (θ) and the wind speed (V) were varied from 0 to 30° and 0.30 to 1.27 m/s, respectively. The surface gas velocity of the fire at various downstream locations was measured using temperature-correlation velocimetry (TCV), which was enabled using streamwise temperature signals from an array of micro-thermocouples. The effect of the slope was converted to an equivalent surface velocity, U_{slope}, following the concept of fire-induced flow over an inclined surface. A momentum analysis was conducted to isolate the coupling effect of slope and wind based on U_{slope}, V, and the mean measured surface gas velocity within the attached flame region, U_{attach}. Finally, a relationship was proposed to predict the mean velocity of the downstream flow using the upstream wind velocity, flame geometry, and the angle of inclination. The proposed relationship enables estimation of downstream heat transfer from a flame to unburnt fuel ahead of the fire, providing a generalized method to evaluate the combined slope and wind effect on heating which drives forward fire spread.

Keywords Slope and wind effect · Temperature-correlation velocimetry · Fire-induced flow · Flow field measurement · Wildland fire spread

List of Symbols

d	Spacing between adjacent thermocouples [m]
D	Streamwise depth of the gas burner [m]
g	Gravitational acceleration [m/s^2]
Gr	Grashof number, $\mathrm{Gr} = g\beta\,(T_{mean} - T_0)(L_f + D/2)^3/\nu^2$ or Eq. 4
L	Spanwise length of the gas burner [m]
L_f	Flame attachment length [m]
I	Fireline intensity [kW/m], $I = Q/L$
Q	Heat release rate of the fire [kW]

Extended author information available on the last page of the article

R	Coefficient of the cross-correlation function, or Eq. 2
Re	Reynolds number, $\mathrm{Re} = \bar{U}\left(L_f + D/2\right)/\nu$
t_s	Sampling time [s]
T_0	Ambient air temperature [K]
T	Gas temperature of the flame [K]
T'	Fluctuating components of the temperature [K]
ΔT_{mean}	Mean gas temperature rise, $\Delta T_{mean} = T_{mean} - T_0$, [K]
T_{mean}	Mean gas temperature [K]
U	Flow velocity [m/s]
$\bar{U}$	Mean flow velocity [m/s]
V	Flow velocity of the wind tunnel [m/s]
x	Downstream location from the burner trailing edge [m]

Greek Symbols

β	Thermal expansion coefficient [K^{-1}]
θ	Angle of inclination [°]
ν	Kinematic viscosity of air [m^2/s]
ρ	Normalized coefficient of the cross-correlation
τ	Time lag between temperature signals [s]

Subscripts

0	Ambient
Attach	Attached flame regime
f	Flame
Slope	Slope effect

1 Introduction

The rate of spread of a wildland fire is strongly influenced by both wind and slope [1, 2]. When exposed to an external wind, a horizontally-spreading fire bends towards the concurrent direction, enhancing both radiative and convective heat transfer between the flame and adjacent unburnt fuel [3]. A similar phenomenon occurs when fire spreads uphill, where both the pressure difference-induced 'Coanda' effect and fire-induced flow 'push' the fire towards the inclined surface [4], resulting in a faster rate of fire spread. Often times, wildland fires occur under the presence of both slope and wind, thus subjecting flames to their coupled effects. Although the individual effect of either wind or slope has been widely examined, work investigating and parameterizing their coupled effect is still limited [5].

At present, most studies combing the effects of slope and wind use the fire rate of spread as an explicit output. Such efforts can be categorized into two main approaches. The first defines a base rate of spread using a horizontal flame isolated from slope and wind effects. Slope and wind effects are then characterized individually against the base rate and added together. Rothermel's [1] empirical fire spread model is a good example, where two additive scalar factors for slope and wind, denoted as φ_s and φ_w, are added to the rate of spread function. Recently, Boboulos et al. [6] proposed a regression model to combine φ_s and φ_w instead of a simple addition. The second approach employs a slope factor, used to

modify the wind-driven fire spread rate, thus incorporating both slope and wind effects [2]. Usually, a vector addition is applied to this method [7], which produced reasonable results except when the wind-induced rate of spread is aligned across the slope.

Although the fire rate of spread has been widely adopted in such analyses, shortcomings exist for practical applications. The rate of spread essentially depends on the heating from the flame and the fuel properties, but the later varies from case to case. Moreover, recent findings [8–10] have shown that convective heat transfer significantly modifies the fire rate of spread. Particularly for fine fuel elements in wildland vegetation, convective cooling is observed to effectively offset heating by thermal radiation until convective heating by contact with flames and hot gasses occurs [9]. Resolving these heat transfer processes could be a more physical and universal approach to model the combined effect of slope and wind. Toward that purpose, corresponding flow field measurements of fires are needed.

Stationary gaseous burner fires present advantages when studying spreading fires, facilitating careful control over the fire and ambient environment as well as allowing for more sophisticated diagnostics used here for flow field characterization. By defining a characteristic flame length (also known as flame base drag or extension length), slope and wind effects can be expressed using non-dimensional parameters, such as the Reynolds number (Re), Froude number (Fr), Grashof number (Gr), Richardson number (Ri), and Byram number [11–13]. Efforts have been made to correlate the flame to surface heat flux using these parameters. For a vertical wall fire, Ahamed and Faeth [14] predicted the fire heat flux to the wall using a modified Gr number. For wind-driven flames, a mixed-convection parameter, $\xi = \mathrm{Gr}/\mathrm{Re}^n$ with n as an empirically fitted constant, has been employed to characterize the downstream heating and burning process [11, 15]. However, approaches that address the combined effects of slope and wind is still lacking.

This study explores the combined effect of slope and wind from the perspective of the flow field along the downstream fuel surface. A gaseous burner was employed to produce stationary fires with fireline intensities ranging from 41 to 123 kW/m. Both the angle of the slope and wind velocity were adjusted during the test, which varied from $\theta = 0$ to 30° and $V = 0.30$ to 1.27 m/s, respectively. A temperature-correlation velocimetry (TCV) technique enabled by an array of thermocouples was then used to derive the flow velocity downstream of the flame. Finally, a momentum analysis was carried out to examine the coupling effect of slope and wind. A generalized relationship was proposed to predict the mean velocity of the downstream flow using the slope, flame geometry and upstream wind velocity. Downstream temperature correlations from the same apparatus have been previously reported in the literature [10, 16]. Together with the current analysis, these data offer temperature and velocity information necessary for estimating convective heat transfer to various downstream fuels.

2 Experimental Setup

Experiments were conducted at the USDA Forest Service Missoula Fire Sciences Laboratory. The test apparatus shown in Fig. 1 consisted of a rectangular sand burner (0.61 × 1.83 m^2), which is mounted flush to a large tilt table (2.5 × 1.83 m^2) with an adjustable angle up to 30°. The surface of the table was made from ceramic fiber insulation board (Super Firetemp). The burner was designed in a modular fashion to have 12 equal sections each

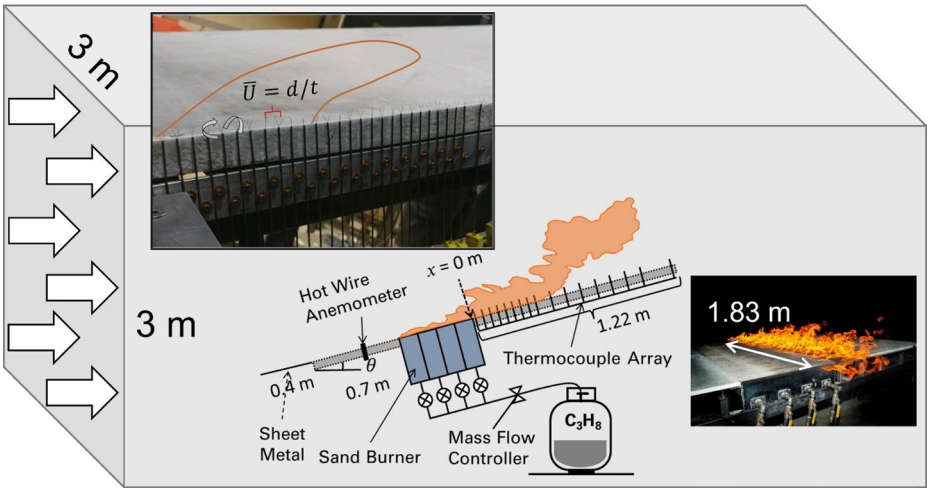

Fig. 1 Schematic and photographs showing the wind tunnel and test apparatus at the USDA Forest Service Missoula Fire Sciences Laboratory used in this study. The top left picture shows the thermocouple layout and below a diagram of the apparatus used for the temperature-correlation velocimetry technique. The bottom right picture shows an example of test

with a 0.15×0.61 m^2 cell size. The resulting aspect ratio of the burner ranges from 1 to 12, with higher aspect ratios helping to simplify the line fires of this study to a 2D problem. Propane was supplied to each section of the burner through a common manifold with independently controlled solenoid valves. Such design allowed for control of the burner surface area and aspect ratios by opening one or more valves. Flow of the propane gas to the manifold was regulated using a mass flow controller (Omega Model FMA-2612 A, $\pm$ 0.8% of reading). A detailed test matrix is summarized in Table 1. Further details on the apparatus is provided in [10].

The entire apparatus was installed in a wind tunnel with a 3×3 m^2 cross-sectional area at the Missoula Fire Sciences Laboratory. The freestream velocity within the wind tunnel was measured continuously using an upstream hot-wire anemometer. To minimize flow separation at the leading edge of the tilt table, a thin 'lip' of sheet metal with a length of 0.4 m was placed upstream of the table surface. Three freestream velocities, 0.30, 0.76, and 1.27 m/s were tested in this experiment. Considering the combined effect of the test apparatus and the slope, the flow velocity ahead of the burner is not necessarily equal to the freestream velocity. Therefore, a hot-wire anemometer was placed 0.3 m upstream of the burner to measure the flow velocity parallel to the table surface. Measurements of the local wind speed near the table surface without the flame were consistent with the wind tunnel freestream flow speed. The fluctuations of the freestream velocity are less than 10%.

A linear array of 60 fine-wire thermocouples (50 μm wire diameter, type-K) elevated 8.5 ± 1.1 mm height above the table surface were deployed along the centerline of the table decking. Spacing between the thermocouples was at 0.01 m for the first 0.3 m, 0.02 m for the next 0.3 m, and then 0.04 m out to 1.2 m. Temperatures were recorded at 500 Hz for 90 s using a National Instruments PXI data acquisition system. Such instrumentation allows for both temperature and flow velocity measurements within the high-temperature region. A TCV technique was employed to derive the local flow velocity.

3 Temperature Correlation Velocimetry

To analyze the combined effect of slope and wind on fire dynamics, local flow velocities are needed. As aforementioned, a hot wire anemometer was employed to measure the cold flow velocity upstream of the flame. However, this technique is incapable of measuring the hot flow velocity within the flaming region. Particle image velocimetry (PIV) has been used to measure the flow field of a flame [17]. However, the large-scale fires in this work make it challenging to seed the flow field and impose a bright enough laser light sheet over the measurement section. In this work, we instead implemented a temperature correlation velocimetry (TCV) technique [18] to measure the flow velocity based on evolution of spatial flow temperature profiles. For flows with a dominant velocity component, such as a turbulent flame or a slug of fluid at a specific temperature, the flow structures are considered to retain their shape and characteristics for a limited time over a given space according to Taylor's 'frozen eddy' hypothesis [19]. It is noted that, compared to laser diagnostics, the TCV method is subject to a relatively higher measurement uncertainty. Cox [20] measured the gas velocity (1 to 5 m/s) of ceiling fire flows, finding a 10% uncertainty compared with pitot tube measurements. A similar 10% uncertainty was also found in the work by Dupuy et al. [21] where they measured the plume velocity of fires from a cylindrical burner. The large scale of experiments provided here have provided exceptional cross-correlation due to the large, turbulent nature of the flames which produce clear temperature peaks for correlation. For example, Fig. 2 displays the measured downstream flow temperatures at different times. It is observed that the flow structures represented by the temperature peaks and troughs propagated to downstream locations at different time steps.

The mean velocity of the flow is then estimated as the weighted average velocity of the surface flow structures, calculated as

$$\bar{U} = d/\tau_{peak}, \tag{1}$$

with d the spacing between two adjacent temperature sensors and τ_{peak} the corresponding traveling time of the flow structure. τ_{peak} was obtained using the cross-correlation function between a pair of temperature signals over a finite time, which is defined as

$$R_{T_i' T_{i+1}'}(\tau) = \frac{1}{t_s}\int_0^{t_s} T_i'(t)\, T_{i+1}'(t+\tau)dt, \tag{2}$$

where i is the i_{th} thermocouple, T_i' and T_{i+1}' are the fluctuating components of the temperature data (i.e., $T' = T - \bar{T}$) and t_s is the sampling time. To minimize the effect of amplitude variations of the temperature fluctuations, a normalized coefficient of the cross-correlation, $\rho_{T_i' T_{i+1}'}$, was further calculated using Eq. 3

Table 1 Experimental conditions for the sand burner

Fireline intensity I [kW/m]	Wind speed V [m/s]	Slope angle θ°	Burner length L [m]	Burner depth D [m]
41, 82, 123	0.30, 0.76, 1.27	0, 6, 12, 18, 24, 30	0.61, 1.22, 1.83	0.15, 0.30, 0.46, 0.61

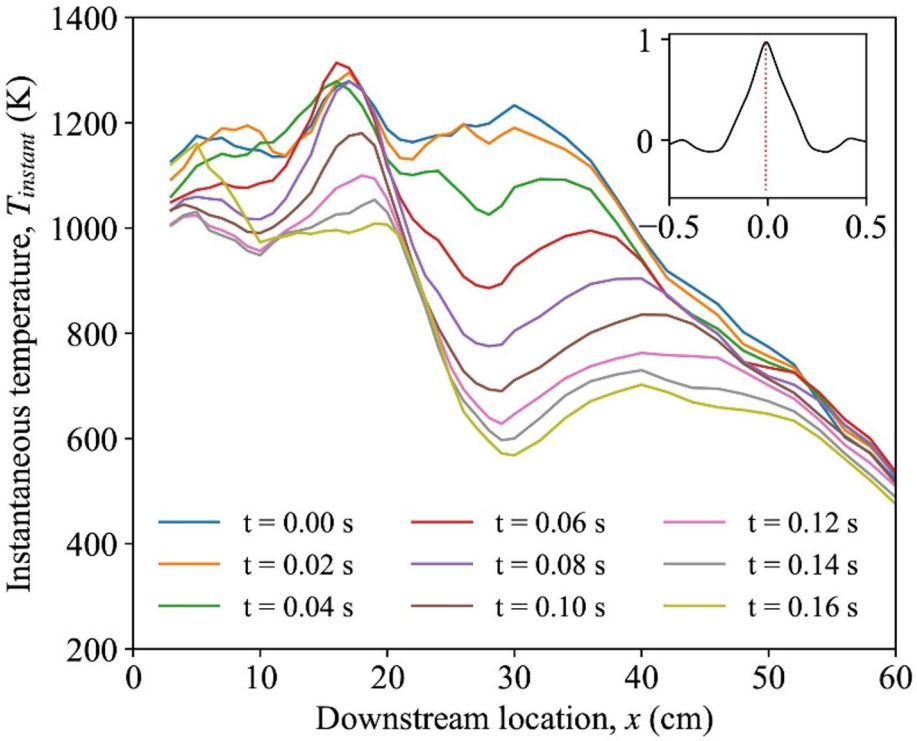

Fig. 2 Instantaneous temperatures downstream of the burner. Measurements were taken under V = 0.76 m/s with θ = 24° and I = 123 kW/m (L = 1.83 m, D = 0.15 m)

$$\rho_{T_i' T_{i+1}'}(\tau) = R_{T_i' T_{i+1}'}(\tau) / \sqrt{R_{T_i' T_i'}(0)\, R_{T_{i+1}' T_{i+1}'}(0)}. \tag{3}$$

The time delay (τ_{peak}) between two similar temperature signals was identified at the peak coefficient of the correlation (see the upper right insert figure in Fig. 2), which was further improved using a sub-sample interpolation method. To ensure an optimal τ, the temperature signals were evaluated with a $t_s = 3$ s (1500 data points) and $t_s = 6$ s (3000 data points) for the attached flame region (see Sect. 4.1) and detached flame region, respectively. Meanwhile, a 0.5 threshold was set for the cross-correlation coefficient ($\rho > 0.5$) to ensure the overall similarity of the temperature signals. During the test, soot deposition occurred on the thermocouple beads, which could add additional uncertainty to the TCV technique. To mitigate such effects, soot was cleaned off thermocouples using a premixed flame or compressed air before each test.

Figure 3 shows an example of the calculated τ and $\bar{U}$ at $x = 20$ cm downstream of the burner ($L = 1.83$ m, $\theta = 24°$). A mean velocity of $\bar{U}$=1.86 m/s was measured with 0.26 m/s root-mean square velocity fluctuations. Note that such fluctuations only reflect part of the turbulent fluctuations since the velocity was smoothed over the spacing between thermocouples. The probability distribution of the velocity appears to take on a lognormal distribution, reflecting the turbulent state of the flow [22].

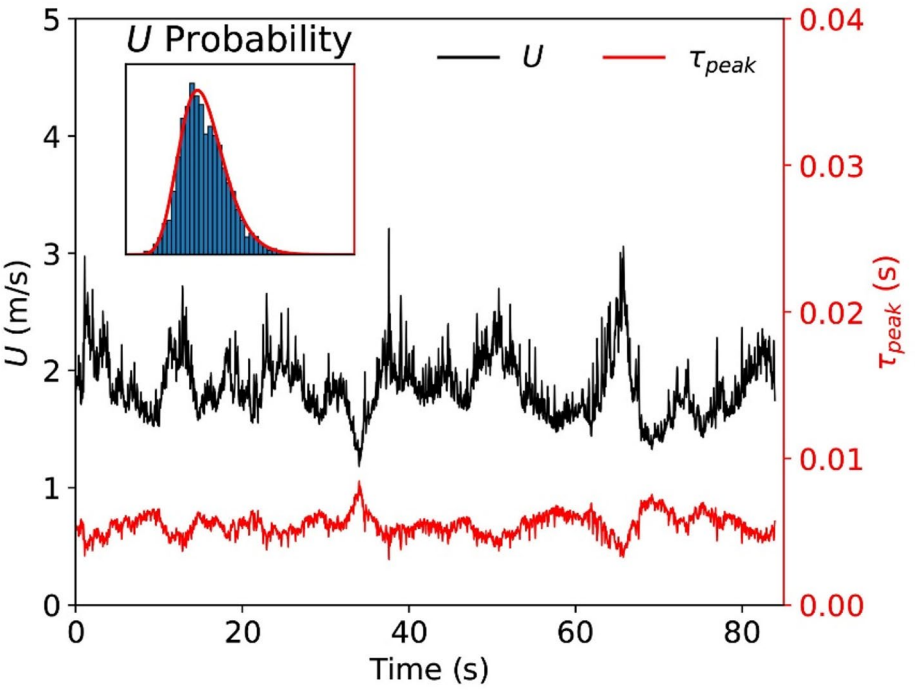

Fig. 3 Calculated flow velocity (U) and time delay (τ_{peak}) vs. time and distribution of the flow velocity (U). Measurements were taken at $x = 20$ cm for a $I = 123$ kW/m fire with a $\theta = 24°$ and $V = 0.76$ m/s ($L = 1.83$ m, $D = 0.15$ m). The data was recorded for 90 s at 500 Hz

4 Results

4.1 Centerline Temperature and Velocity

Due to the limited accessibility of the wind tunnel and the relatively large heat release rate of the flame, images of the flame were not taken. Flame geometry changes were captured through the centerline temperature rise (ΔT_{mean}) above ambient (298 K) displayed in Fig. 4. For a fixed freestream velocity, at $V = 0.3$ m/s, a lower temperature rise above the ambient was measured with $\theta \leq 12°$, as displayed in Fig. 4a. The flame geometry here was primarily dominated by the vertical component of the buoyancy. Radiation then dominated the heat transfer from the flame to downstream locations under this angle. While for $\theta > 12°$, the temperature rise reached $\sim$1000 K at the initial downstream locations, indicating that flame was attached to the downstream surface, and thus occurred in a mixed-convection heat transfer region. Further increases in θ elongated the length of this region up to the location marked as ' $\times$ ', which represents the flame extension length [16]. Similarly, Fig. 4b shows that a higher freestream velocity altered the flame from a detached state to an attached state for $\theta = 12°$. This is as expected since both the slope and the wind tend to 'push' the buoyant-driven vertical flame closer towards the downstream surface.

With the help of the TCV, local flow velocities of the flames were derived and plotted in Fig. 5 to better understand the flow dynamics. For $V = 0.30$ m/s, the direction of the

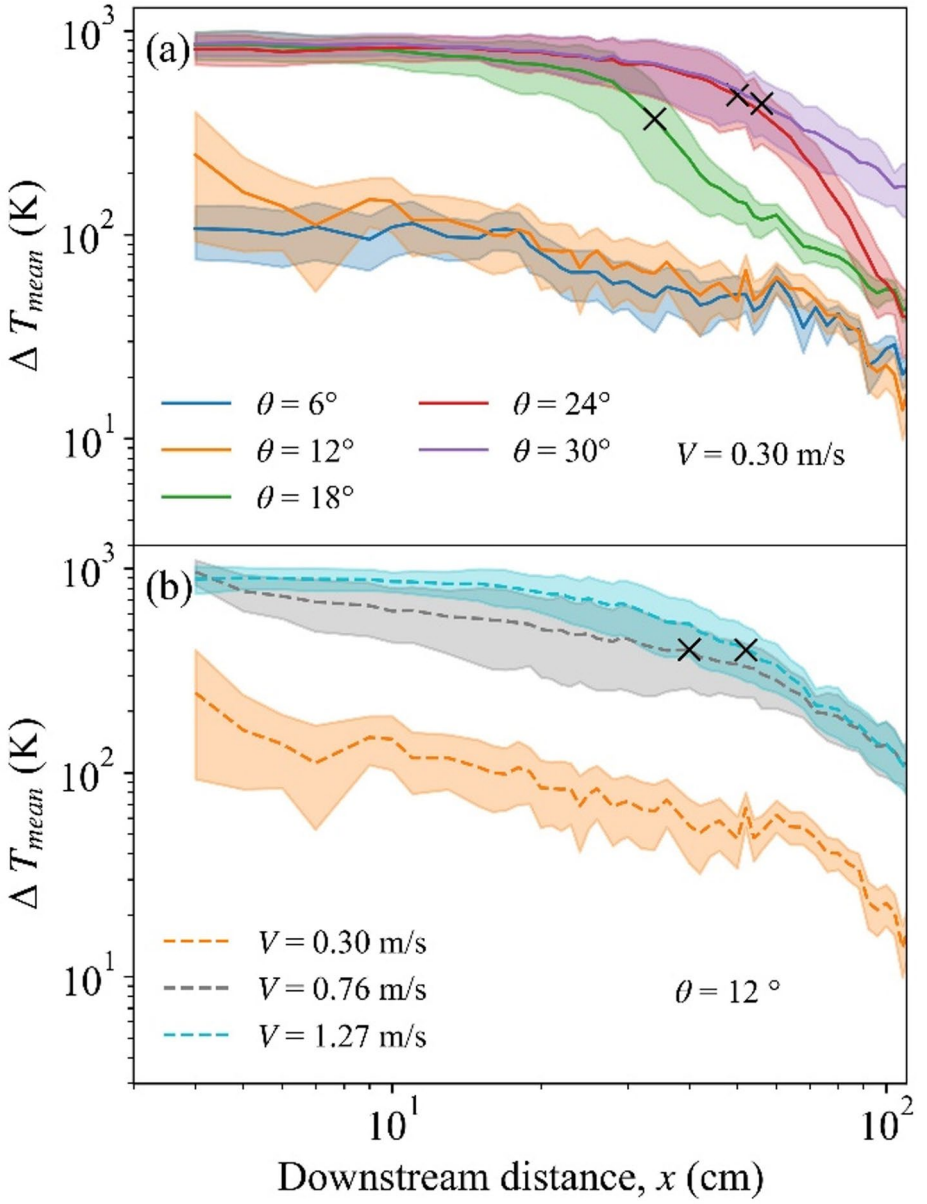

Fig. 4 Mean temperature rise (ΔT_{mean}) vs. downstream distance (x): (a) various angles of inclination (θ) with a fixed freestream velocity ($V = 0.3$ m/s), (b) various V with a fixed $\theta = 12°$. The shaded areas represent the standard deviation of the mean. Measurements were taken for a $I = 123$ kW/m fire with burner size $L = 1.83$ m and $D = 0.15$ m

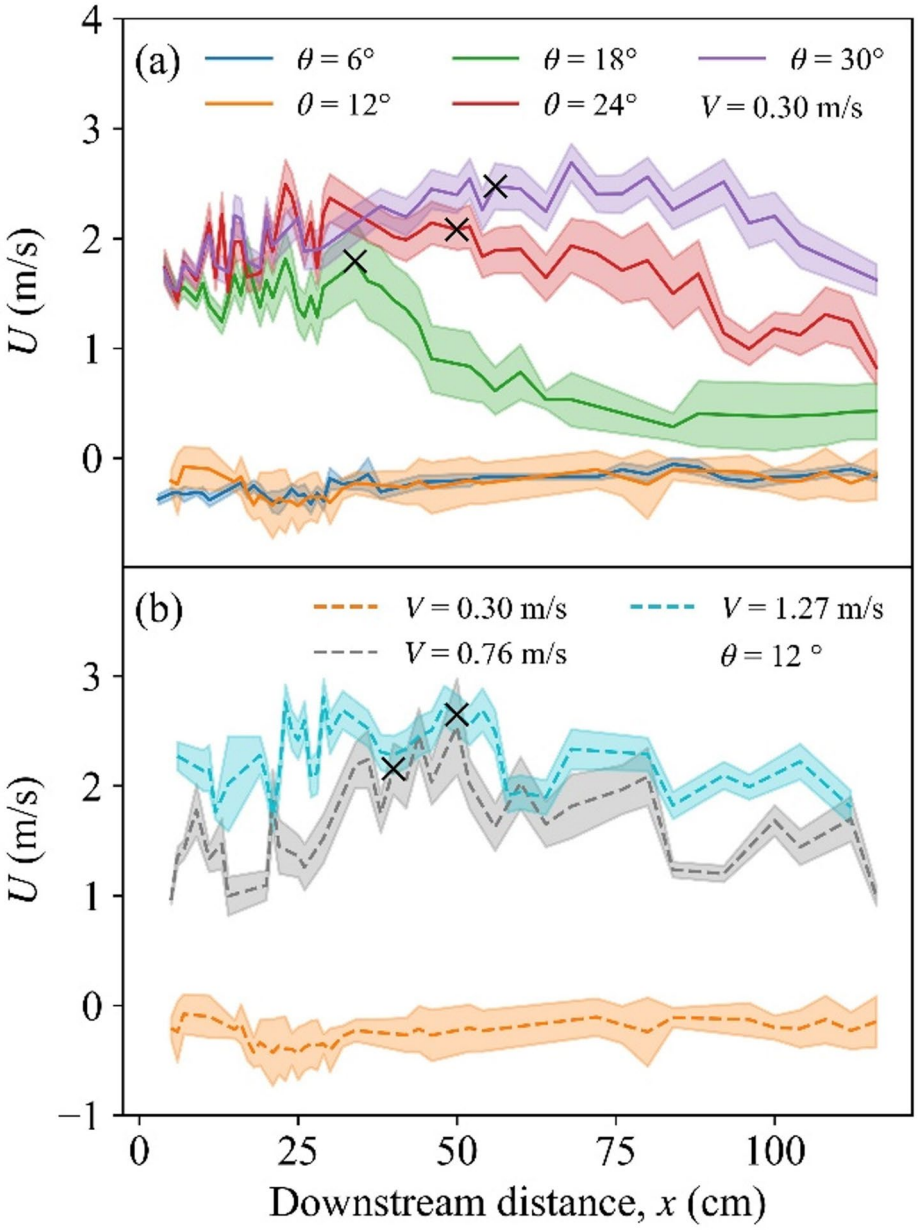

Fig. 5 Surface flow velocities (U) vs. downstream distance (x): (a) various angles of inclination (θ) with a fixed freestream velocity ($V = 0.3$ m/s), (b) various V with a fixed $\theta = 12°$. The shaded areas represent 1/2 of the standard deviation. Measurements were taken for a $I = 123$ kW/m fire with burner size $L = 1.83$ m and $D = 0.15$ m

flow reversed at $12° < \theta < 18°$. At an angle of 6 to 12°, a steady negative velocity was measured, indicating an opposed flow toward the flame base driven by the entrained air. Such results agree with temperature measurements, which show that the flame was similar to a vertical buoyancy driven flame. For angles between 18 and 30°, the flow velocity at the downstream location increased to a peak then slowed down. The initial acceleration is likely driven by the buoyancy component along the inclined surface arising from the attached flame region (marked as ' × '). Once the flame detached at a downstream location, a peak velocity was reached and the flow velocity started to slow down afterwards. Again, similar velocity profiles were observed in Fig. 5b for conditions with a lower angle of inclination but higher freestream velocities. In other words, the slope and wind have interchangeable effects on downstream flow velocities.

4.2 Coupled Slope-Wind Effect

Flow measurements show that both slope and wind change the flow structure and accelerate the downstream flow within the attachment region. A method to quantify their combined effect, however, has not yet been developed. A force diagram is plotted in Fig. 6 to decompose this physical process, where F_{buoy} represents the fire-induced buoyancy force, $F_{buoy,p}$ represents the component of buoyant force parallel to the slope, and $F_{buoy,n}$ represents the component normal to the slope. The most direct outcome of the combined slope and wind effect is that the extension of the flame (L_f) exceeds the burner trailing edge (D). Both high temperatures and velocities were measured within this extension length, which is defined as the characteristic flame attachment length, L_f (measured at $T_{mean} = 798$ K), similar to literature results [10, 16]. This extended fire region acts as the 'hot plate' in natural convection flow and changes the magnitude of the flow. According to Umemura and Law [4], for sufficiently large values of Gr_{L_f}, a boundary layer is developed over the plate. The

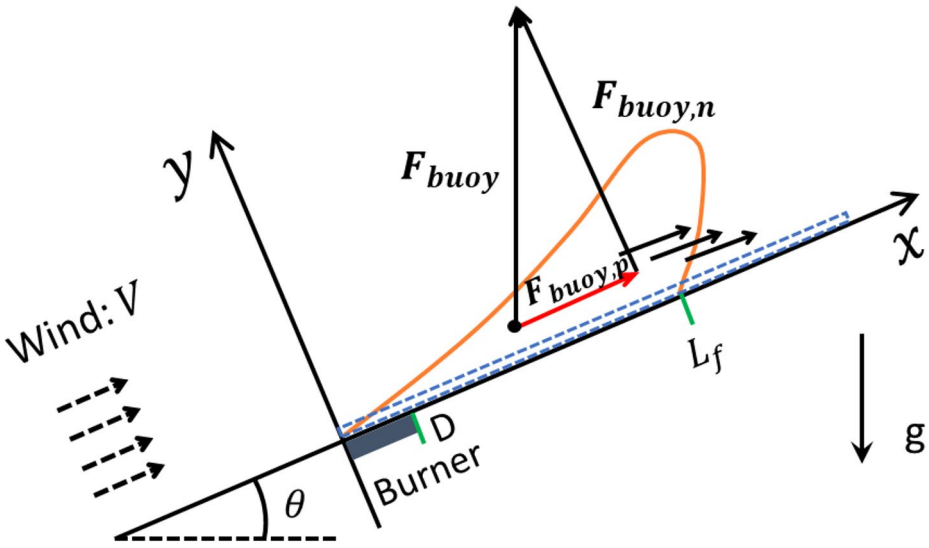

Fig. 6 Diagram of the combined slope and wind effect

buoyancy effect of the fire, F_{buoy}, can be quantified using the Grashof number (Gr), which is calculated as:

$$\mathrm{Gr} = g\beta\,(T_{mean} - T_0)(L_f + D/2)^3/\nu^2, \tag{4}$$

with g the standard acceleration due to gravity, β the air's coefficient of thermal expansion ($\beta \approx 1/T_{mean}$), T_0 the ambient air temperature, D the burner streamwise depth and ν the kinematic viscosity of air. The slope effect ($F_{buoy,p}$) is the component of the fire-induced buoyant force (F_{buoy}) along the inclined surface, defined as $\mathrm{Gr}\sin\theta$. To facilitate the latter comparison, $F_{buoy,p}$ is further converted to momentum using the analogy $\mathrm{Gr}\sin\theta \sim \mathrm{Re}^2$, where $\mathrm{Re} = U(L_f + D/2)/\nu$. Assuming full conversion of buoyant force to momentum, we set $\mathrm{Gr}\sin\theta = \mathrm{Re}^2$. Rewriting this relationship using Eq. 4, we have $g\beta\,(T_{mean} - T_0)(L_f + D/2)^3/\nu^2\sin\theta = U^2(L_f + D/2)^2/\nu^2$. The buoyancy-induced velocity U_{slope} is then derived as $U_{slope} = \sqrt{gA(L_f + D/2)sin\theta}$, with $A = 1 - T_0/T_{mean}$. The external wind effect is a known factor, denoted as V. The measured combined effect of the buoyancy-induced flow and external wind was calculated as the mean flow velocity within the attached flame region, denoted as U_{attach}. To evaluate the role of U_{slope} and V, ratios representing their contributions to U_{attach} were calculated as

$$R_1 = U_{slope}/U_{attach}, \tag{5}$$

and

$$R_2 = V/U_{attach}. \tag{6}$$

Figure 7a displays the results under a $V = 0.3$ m/s external wind. Note that each data point in Fig. 7 represents the averaged value across different burner aspect ratios. During the surface flow velocity measurements, no clear correlation between burner aspect ratio and surface flow velocity was observed. It is observed that the majority of the downstream flow is attributed to the fire-induced flow due to slope. External wind played a secondary role for all slopes tested. When the freestream velocity increased to V = 0.76 m/s, the external wind dominated the flow at lower angles of inclination, as displayed in Fig. 7b. As the slope increased to 12° ∼ 18°, the fire-induced flow and the external wind together contributed to the overall downstream flow. After 18°, the slope effect exceeded the wind effect. Similar results (see Fig. 7c) were obtained for V = 1.27 m/s, except that the external wind played a larger role until an angle around 24°. This is expected as the external wind does not depend on the fire geometry, and thus outperforms the slope effect when having a higher wind speed. Overall, for most of the slopes and wind speeds tested, the values of R_1 and R_2 are less than 1, affirming the existence of a combined effect.

To evaluate this combined effect, two methods are proposed. The first one is a simple scalar addition of velocities, i.e., $R_{comb,\,1} = R_1 + R_2$. The second method is an addition of the corresponding momentum induced by the slope ($U_{slope}{}^2$) and the wind (V^2), calculated as

$$R_{comb,\,2} = \sqrt{U_{slope}{}^2 + V^2}/U_{attach}. \tag{7}$$

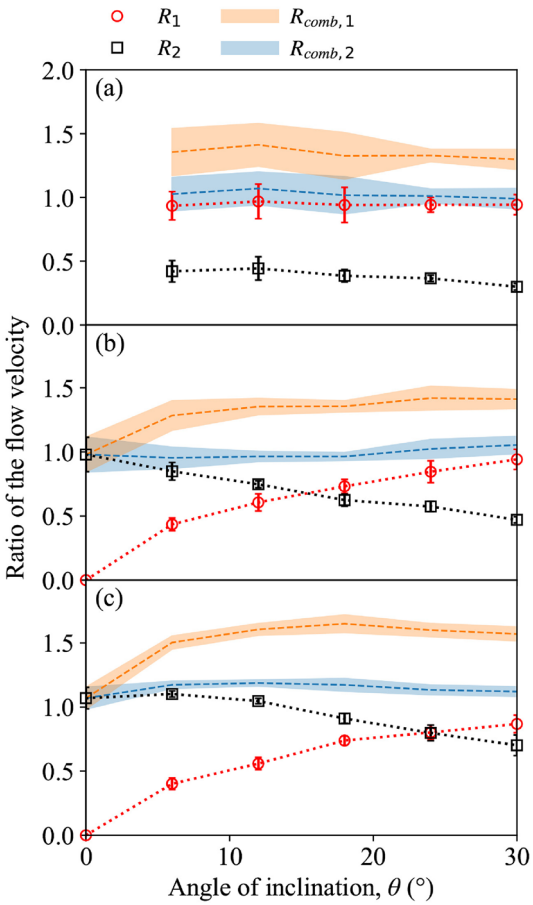

Fig. 7 Ratios of the velocity components vs. angles of inclination: **a** V = 0.30 m/s, **b** V = 0.76 m/s and **c** V = 1.27 m/s. The error bars and shaded areas represent the standard deviation of the mean among various burner length (L: 0.61, 1.22 and 1.83 m) and depth (D: 0.15, 0.30, 0.46, 0.61 m)

The resulting $R_{comb,\ 1}$ and $R_{comb,\ 2}$are displayed in Figs. 7a–c. Ideally, the contributions of slope and wind should collectively represent the balance between the combined slope-wind effect and the measured actual flow behavior, under the assumption that the slope contribution follows the relation $\mathrm{Gr}sin\theta\ = \mathrm{Re}^2$, thereby yielding a ratio close to one. The values of $R_{comb,\ 1}$ range from 1.35 to 1.60 for most of the conditions, meaning that the velocity addition approach overestimates the combined slope and wind effect. On the other hand, values of $R_{comb,\ 2}$ range from 0.96 to 1.13, supporting the concept of balanced momentum between the downstream flow and the combined slope and wind effect. Although the slope-driven and wind-driven flows are aligned in the same downstream direction, experimental data indicate that their contributions do not combine linearly. Instead, a momentum-based addition better captures the interaction between these effects, suggesting a plausible way of incorporating their effects from the flow field perspective.

4.3 A Generalized Relationship for Combined Slope-Wind Effect

With $U_{slope} = \sqrt{gA(L_f + D/2)sin\theta}$, using $R_{comb,\ 2}$ = 1, Eq. 7 can be re-written as

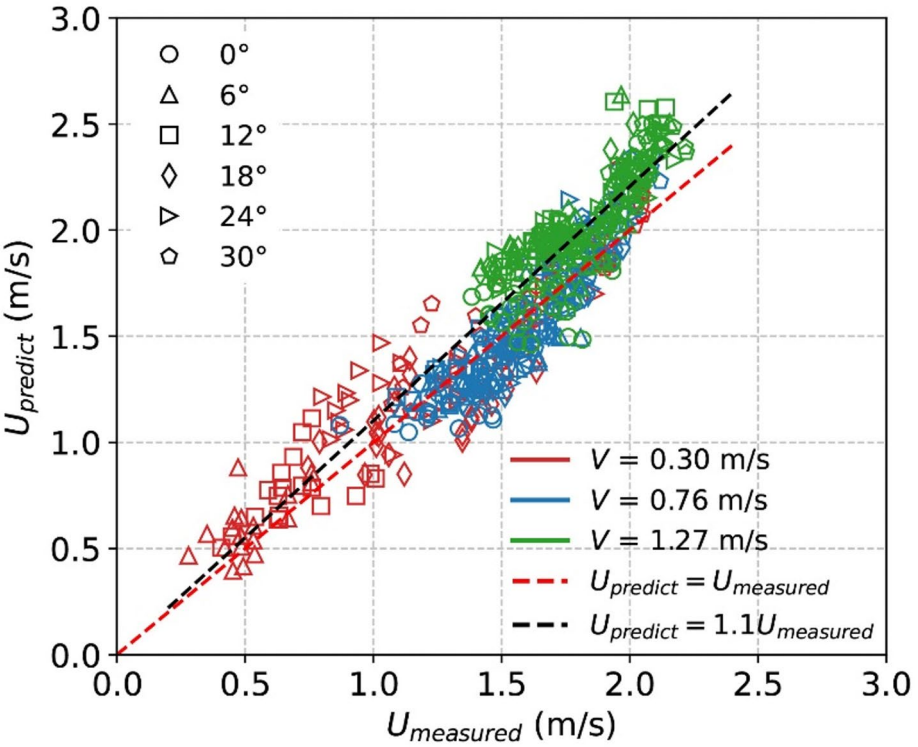

Fig. 8 Predicted downstream flow velocity vs. measured downstream flow velocity. Burner length (L) ranges from 0.61 to 1.83 m, depth (D) ranges from 0.15 to 0.61 m

$$U_{predict} = \sqrt{{U_{slope}}^2 + V^2} = \sqrt{gA(L_f + D/2)sin\theta + V^2}, \tag{8}$$

where $U_{predict}$ is the predicted flow velocity in the flame attachment region. Equation 8 suggests that the downstream surface flow velocity can be calculated once knowing the slope, wind velocity, and flame geometry, which is commonly available for practical fires or modeling processes. Figure 8 plots the predicted velocity using Eq. 8 against the measured downstream velocity. In general, the proposed method predicts the downstream flow velocity well with a 10% overprediction on average. This relationship enables estimation of the hot gas velocity within the attached flame regime under the combined effect of slope and wind. Convective heat transfer from the flame to the downstream surface can therefore be better predicted, enabling a physically-based estimation of the rate of fire spread for different fuels. It is noted that the relationship here is limited to a surface flow velocity comparison.

4.4 Discussion

In wildland fire scenarios, slope, wind, and their coupled effect strongly affects the heat transfer from flames to unburnt fuels. The role of convective heating has been highlighted since wind and slope-driven wildland fires are seen to be driven by direct flame contact [9, 10]. The rate of fire spread, as a strong function of local flow, fuel size, relative humidity,

and other parameters, is not suitable for generalized studies regarding the combined slope and wind effect. The flow velocity ahead of the flame, on the other hand, is of importance to evaluate the heat transfer process. This is especially true for fine fuel elements, whose ignition strongly depends on the rate of convective heat transfer and are known to drive fire spread [23]. This work provides insight into the flame flow field under the combined slope and wind effect.

In reality, both slope and wind are directional where vector addition of the velocity components need to be adopted. Although the slope and wind measured in this work have the same direction relative to the surface, the TCV technique can also measure the velocity of directional flows. A framework based on this study could be further extended to more complex directional flow measurements in fire.

5 Conclusion

Slope and wind often coexist in wildland fires, but few studies have quantified their effect on fire spread. This work explores the coupled slope and wind effect to fires from a flow field perspective. Various angles of inclination (θ) and external wind velocities (V) were introduced. The effect of the slope was further converted to a fire-induced flow velocity, U_{slope}. The local flow velocity downstream of the flame, U_{attach}, was measured using a TCV technique. The results show that the coupling effect of the slope and wind follows a momentum balance theory, meaning ${U_{attach}}^2 = {U_{slope}}^2 + V^2$. Finally, an empirical relationship was proposed to predict the mean velocity of the downstream flow using the upstream wind velocity, flame geometry, and the angle of inclination. This work serves as a first step to quantify the combined slope and wind effect account for changes in the downstream flow velocity. The obtained velocity information could be further used to evaluate the convective heat transfer from the flame to the unburnt fuel and compared to fire spread measurements.

Acknowledgements The authors would like to acknowledge financial support for this work from the National Science Foundation through CBET award 1554026 and from the USDA Forest Service Rocky Mountain Research Center through the National Fire Decision Support Center. The authors would like to sincerely thank Josh Deering, Andrew Gorris, Jon Bergroos, and Randy Pryhorocki at the Missoula Fire Sciences Laboratory for their support in developing the experimental apparatus and help in conducting the experiments.

Open Access This article is licensed under a Creative Commons Attribution 4.0 International License, which permits use, sharing, adaptation, distribution and reproduction in any medium or format, as long as you give appropriate credit to the original author(s) and the source, provide a link to the Creative Commons licence, and indicate if changes were made. The images or other third party material in this article are included in the article's Creative Commons licence, unless indicated otherwise in a credit line to the material. If material is not included in the article's Creative Commons licence and your intended use is not permitted by statutory regulation or exceeds the permitted use, you will need to obtain permission directly from the copyright holder. To view a copy of this licence, visit http://creativecommons.org/licenses/by/4.0/.

References

1. Rothermel RC (1972) A mathematical model for predicting fire spread in wildland fuels. Res. Pap. INT-115, vol 115. U.S. Department of Agriculture, Intermountain Forest and Range Experiment Station, Ogden, UT, p 40

2. Sharples JJ (2008) Review of formal methodologies for wind - slope correction of wildfire rate of spread. Int J Wildland Fire 17:179–193. https://doi.org/10.1071/wf06156
3. Ren X, Ju X, Gollner MJ (2022) Effect of freestream turbulence on the structure of boundary-layer flames. Combust Flame 236:111750. https://doi.org/10.1016/j.combustflame.2021.111750
4. Umemura A, Law CK (1990) Natural-convection boundary-layer flow over a heated plate with arbitrary inclination. J Fluid Mech 219:571–571. https://doi.org/10.1017/s0022112090003081
5. Gollner MJ, Miller CH, Tang W, Singh AV (2017) The effect of flow and geometry on concurrent flame spread. Fire Saf J 91:68–78. https://doi.org/10.1016/j.firesaf.2017.05.007
6. Boboulos M, Purvis MRI (2009) Wind and slope effects on ROS during the fire propagation in East-Mediterranean pine forest litter. Fire Saf J 44:764–769. https://doi.org/10.1016/j.firesaf.2009.03.006
7. McArthur AC (1966) Weather and grassland fire behavior, Department of national Development, Forestry and Timber Bureau Leaflet No. 100. Canberra, ACT
8. Finney MA, Cohen JD, McAllister SS, Jolly WM (2013) On the need for a theory of wildland fire spread. Int J Wildland Fire 22:25. https://doi.org/10.1071/wf11117
9. Finney MA, Cohen JD, Forthofer JM et al (2015) Role of buoyant flame dynamics in wildfire spread. Proc Natl Acad Sci 112:9833–9838. https://doi.org/10.1073/pnas.1504498112
10. Finney MA, Grumstrup TP, Grenfell I (2020) Flame characteristics adjacent to a stationary line fire. Combust Sci Technol 194:2212–2232. https://doi.org/10.1080/00102202.2020.1863952
11. Ju X, Gollner MJ, Wang Y et al (2019) Downstream radiative and convective heating from methane and propane fires with cross wind. Combust Flame 204:1–12. https://doi.org/10.1016/j.combustflame.2019.03.001
12. Tang W, Miller CH, Gollner MJ (2017) Local flame attachment and heat fluxes in wind-driven line fires. Proc Combust Inst 36:3253–3261. https://doi.org/10.1016/j.proci.2016.06.064
13. Byram G (1959) Combustion of forest fuels. In: davis KP (ed) Forest fire control and use. McGraw-Hill, New York, pp 90–123
14. Ahmad T, Faeth GM (1979) Turbulent wall fires. Proc Combust Inst 17:1149–1160. https://doi.org/10.1016/s0082-0784(79)80109-5
15. Singh A, Singh AV (2021) Burning behavior of mixed-convection wind-driven flames under varying freestream conditions. Fire Saf J 122:103320. https://doi.org/10.1016/j.firesaf.2021.103320
16. Ren X, Sluder ET, Heck MV et al (2022) Scaling analysis of downstream heating and flow dynamics of fires over an inclined surface. Combust Flame 242:112203–112203. https://doi.org/10.1016/j.combustflame.2022.112203
17. Morandini F, Silvani X, Dupuy J-L, Susset A (2018) Fire spread across a sloping fuel bed: flame dynamics and heat transfers. Combust Flame 190:158–170. https://doi.org/10.1016/j.combustflame.2017.11.025
18. Belyaev IA, Razuvanov NG, Sviridov VG et al (2017) Temperature correlation velocimetry technique in liquid metals. Flow Meas Instrum 55:37–43. https://doi.org/10.1016/j.flowmeasinst.2017.05.004
19. Taylor GI (1938) The spectrum of turbulence. Proceedings of the Royal Society, Mathematical A. Proc R Soc Lond A Math Phys Sci 164:476–490. https://doi.org/10.1098/rspa.1938.0032
20. Cox G (1977) Gas velocity measurement in fires by the cross-correlation of random thermal fluctuations-a comparison with conventional techniques. Combust Flame 28:155–163. https://doi.org/10.1016/0010-2180(77)90021-9
21. Dupuy J-L, Maréchal J, Morvan D (2003) Fires from a cylindrical forest fuel burner: combustion dynamics and flame properties. Combust Flame 135:65–76. https://doi.org/10.1016/s0010-2180(03)00147-0
22. Miller CH, Tang W, Sluder E et al (2017) Boundary layer instabilities in mixed convection and diffusion flames with an unheated starting length. Int J Heat Mass Transf 118:1243–1256. https://doi.org/10.1016/j.ijheatmasstransfer.2017.11.040
23. Cohen JD, Finney MA (2010) An examination of fuel particle heating during fire spread, in: In: Viegas, DX, ed. Proceedings of the VI International Conference on Forest Fire Research. Coimbra, Portugal

Publisher's Note Springer Nature remains neutral with regard to jurisdictional claims in published maps and institutional affiliations.

Authors and Affiliations

Xingyu Ren[1,2] · Evan T. Sluder[1,4] · Michael V. Heck[1] · Torben P. Grumstrup[3] · Mark A. Finney[3] · Simo A. Mäkiharju[2] · Michael J. Gollner[1,2]

✉ Michael J. Gollner
mgollner@berkeley.edu

Xingyu Ren
xyren@terpmail.umd.edu

Evan T. Sluder
esluder@ibhs.org

Michael V. Heck
mike_hck55@yahoo.com

Torben P. Grumstrup
torben.p.grumstrup@usda.gov

Mark A. Finney
mark.finney@usda.gov

Simo A. Mäkiharju
makiharju@berkeley.edu

[1] Department of Fire Protection Engineering, University of Maryland, 4356 Stadium Dr., College Park, MD 20742-3031, USA

[2] Department of Mechanical Engineering, University of California, Berkeley, 6105A Etcheverry Hall, Berkeley, CA 94720-1740, USA

[3] Missoula Fire Sciences Laboratory, US Forest Service, 5775 US Highway 10 W, Missoula, MT 59808-9361, USA

[4] Insurance Institute for Business & Home Safety, 5335 Richburg Rd, Richburg, SC 29729, USA